Research Article

Substrate free ultrasonic-assisted hydrothermal growth of ZnO nanoflowers at low temperature

Anu Katiyar[1] · Nishant Kumar[1] · R. K. Shukla[1] · Anchal Srivastava[1]

Received: 2 April 2020 / Accepted: 6 July 2020 / Published online: 16 July 2020

Abstract
ZnO nanoflowers (NFs) have been synthesised using a simple cost effective ultrasonic-assisted hydrothermal method at low temperature of 95 °C. Here the NFs consist of petal-like arrangement of several hexagonal-shaped nanorods, the length and diameter of which lie in a range of 100–150 nm and 30–70 nm, respectively. ZnO NFs possess hexagonal wurtzite phase, high crystallinity and strong absorption in the UV region. The optical band gap 3.25 eV of these NFs estimated by two different ways is found to be nearly the same. Room temperature photoluminescence spectrum reveals that the ZnO NFs exhibit dominant UV emission and three major emissions in the visible i.e. violet, blue–green and yellow. NFs are promising nanostructures for application in environment related sensors and antimicrobial activity.

Keywords Zinc oxide · Nanoflowers · Ultrasonic · Defect emission

1 Introduction

Zinc oxide (ZnO) is a versatile functional material which is chemically stable, non-toxic and environment friendly. ZnO exhibits excellent properties such as wide band gap (3.37 eV), large exciton binding energy (60 meV), high transparency, high electron mobility and strong room temperature photoluminescence [1, 2]. As ZnO nanoparticles also show antimicrobial activity they are being impregnated into textile fibers for mask preparation in the current difficult times of COVID-19 pandemic. Hexagonal wurtzite structure of ZnO facilitates a diverse group of morphological nanostructures such as nanorods, nanowires, nanotubes, nanocombs, nanosprings, nanocages, nanohelices, nanoflowers (NFs) etc. [3–5]. These extraordinary properties of ZnO, make it one of the most studied material in nanotechnology. Nanostructured ZnO is currently receiving attention for device fabrication also due to its superior physical and chemical properties. Gas sensing and photocatalytic activity of ZnO nanostructures can be tuned by varying its morphology [6]. A variety of methods have been adopted for the synthesis of nano/micro structured ZnO such as: hydrothermal method for ZnO NFs [6–10], microwave-assisted hydrothermal method for the growth of ZnO nano/micro structures [11], citric acid-assisted hydrothermal method for flower-like ZnO nanostructures [12], modified sol–gel method and solution plasma method for ZnO NFs [13], ultrasonic-assisted co-precipitation method for nanosheet based ZnO hierarchical structure [14] and ultrasonic-assisted hydrothermal method for flower-like nano ZnO [7], Ga doped ZnO nanorods [15], alpha-FeOOH flowers [16] and ZnO microstructures [17]. Hydrothermal method has also been used for the growth of ZnO nanoflowers on Si [18] and FTO [19] substrate. Ultrasonic treatment affects the morphology and facilitates the crystallization of ZnO. It has been reported that the ultrasonic treatment induces acoustic cavitation in liquid which forces many kinds of chemical reactions that may not take place otherwise viz. homogenous dispersion of species such as zinc ion, decomposition of H_2O into $H^{\cdot}$ and $OH^{\cdot}$ radicals etc. [7].

✉ Anchal Srivastava, asrivastava.lu@gmail.com | [1]Department of Physics, University of Lucknow, Lucknow 226007, India.

Flower-like ZnO nanostructures render excellent performance in gas sensing and photocatalytic degradation due to high surface area and large surface defects [8, 20]. Exhibition of superior photocatalytic activity in the degradation of Rhodamine B is one such example [21]. The ZnO NFs assembled by nanoplates exhibited the better gas-sensing performance as compared to the nanoparticles and nanoplates due to high specific area and abundant spaces for gas diffusion [9]. The hydrothermal growth of ZnO NFs into teflon-lined stainless steel autoclave in the temperature range 100–200 °C is most widely reported [6–10, 17, 20, 22]. The Teflon-lined stainless steel autoclave is quite expensive. A simple, cost effective, synthesis of ZnO nanostructures at low temperature avoiding toxic/hazardous chemicals or by-products is most challenging. For this reason, we have demonstrated the hydrothermal growth of ZnO nanostructures in a low-cost Borosil autoclave bottle at low-temperature (95 °C).

Herein, flower-like ZnO nanostructure has been grown by ultrasonic-assisted hydrothermal method without the assistance of any template, substrate or seed layer and elucidated in terms of their structural, morphological, optical and photoluminescence properties. Such NFs due to their increased surface area are promising nanostructures for application in the field of environment related devices, inhibitor to *E. Coli* bacteria, non-enzymatic glucose sensor [23]. The morphologies and surface area of the ZnO nanomaterials are reported to have a strong impact on the antibacterial properties as the catalysis of radical formation occurs on the nanomaterials surfaces [23, Ref. 9, 15 cited therein].

2 Experimental

A schematic diagram describing step-wise synthesis of ZnO NFs using ultrasonic-assisted hydrothermal method is shown in Fig. 1. In a typical synthesis process, 0.1 M solutions of zinc nitrate hexahydrate [$Zn(NO_3)_2{\cdot}6H_2O$, (99.99% pure, SD Fine Chem. Ltd.)] and hexamethylenetetramine [HMT($C_6H_{12}N_4$), (99.50% pure, Merck KGaA, Germany)] were prepared separately in deionized water using magnetic stirring for 30 min and named as solution A and solution B, respectively. Solution B was added drop wise in the solution A and mixed through a sonication process in ultrasonic water bath (Ultrasonic cleaner, LABMAN-40 kHz) at 50 °C for 30 min. The sonicated solution (A + B) was magnetically stirred and aged for 3 h at room temperature to achieve a homogenous solution. For hydrothermal reaction, the obtained solution was transferred to autoclave bottle, sealed and maintained at 95 °C for 4 h in muffle furnace. Then the autoclave bottle was naturally cooled to room temperature. A white precipitate settled at the bottom of the autoclave bottle. The supernatant solution was separated carefully and remaining white precipitate was washed three times with deionised water and ethanol to remove possible impurities and then dried in air at 60 °C.

The successfully synthesized ZnO sample was characterized for its surface morphology and size using FESEM (Model-JEOL) for an accelerating voltage of 25 kV and 14.40 mm working distance. The crystallographic and structural properties were studied using X-Ray diffractometer (Model-Rigaku Ultima IV) for 2θ values ranging

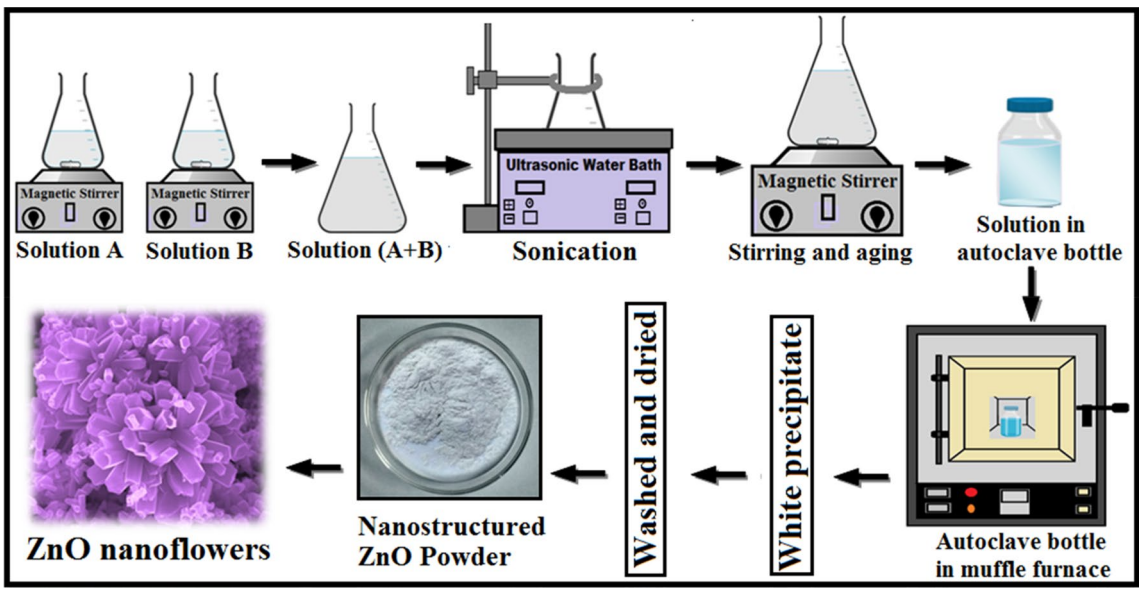

Fig. 1 Schematic diagram for the ultrasonic-assisted hydrothermal growth of ZnO NFs

from 20° to 90° using CuK_{α} radiation (λ = 1.540598 Å). The absorption spectrum has been recorded using UV–Vis spectrophotometer (Model-V670, Jasco). The photoluminescence spectrum has been recorded using fluorescence spectrometer (Model LS-55, Perkin Elmer) for excitation wavelength 325 nm obtained from a 20 kilowatt xenon discharge lamp. All these measurements have been done at room temperature.

3 Results and discussion

3.1 Surface morphology

The surface morphology of the synthesized ZnO sample is shown in Fig. 2. The FESEM image reveals the formation of flower-shaped ZnO nanostructure assembled with radially oriented nanorods. Notable thing is that the NFs are constituted by the accumulation of several hexagonal-shaped nanorods. The length and diameter of individual nanorods are estimated to be about 100–150 nm and 30–70 nm, respectively. The ZnO nanorods arrangement is like flower-petals originating from the centre in such a spherical shape that they exhibit perfect flower-like morphology. It is observed that each flower is flanked by many other flowers on all sides indicating a high yield of NFs during synthesis. Also during the FESEM analysis at low magnification, we had observed the morphology of the entire sample at different locations and found that whole sample is adorned with the flower-like structure. The chemical methods provide large yields as compared to the physical methods because there is no loss of reactants during chemical reaction.

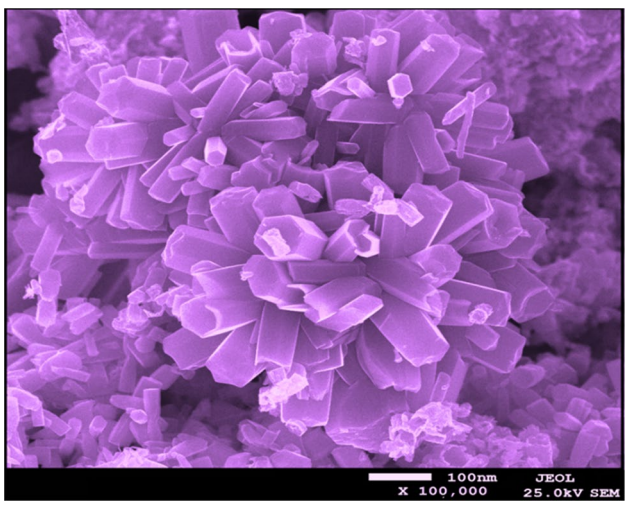

Fig. 2 FESEM image of the ZnO NFs

The basal polar plane (0001) of ZnO has surface energy higher compared to the non-polar {0110} and {2110} planes and this leads to anisotropic growth. In thermodynamic equilibrium the facet with higher surface energy has smaller area and therefore growth along c-axis is favored for ZnO [24]. However, an excess of OH^- restrains such growth and fuels the sideways growth resulting in nanosheets. Thus the solvent providing hydroxide ions affects the growing nanostructure. Under hydrothermal condition, growth of ZnO crystals depends upon direction and is maximum for (0001) [25] especially in the presence of HMT which acts as a shaping surfactant also besides being buffer. Nanorods with hexagonal cross-section arise to minimize the surface energy by maintaining the crystal structures. When the growing phase boundaries touch each other, a base structure is formed and growth along radial direction predominates leading to nano-rods-flower-like structures [26].

The nano-rods-flower morphology obtained here is expected to show better photocatalytic property as compared to that shown by nano-sheets-flower because nanorods, being one dimensional nanostructure exhibit superior electrochemical properties due to their dimensional anisotropy i.e. due to the presence of zinc terminated and oxygen terminated polar facets with high surface energy. Also the larger surface area of hexagonal rods increases the number of electron and holes on the active sites which exists on the surface, resulting in higher activity [27]. Similar finding about graphitic carbon nitride is reported in literature [28] where photocatalytic activity and photocurrent for nanorods under visible light were approximately 1.5 and 2.0 times respectively as compared to those for nanoplates. This was again due to increase in active lattice facets.

Some nanoflowers reported in literature are mentioned here. ZnO NFs having petals with length and width 200–400 nm and 100–200 nm, respectively composed of assemblies of smaller nanocrystallites have been synthesized on Si substrate by the hydrothermal method [18]. ZnO NFs constitute of nanorods having length and diameter about 234–347 nm and 77–106 nm, respectively had been synthesized by the hydrothermal process [6]. The flower-like ZnO materials composed of interacted nanosheets with an average thickness of 5 nm had been synthesized by solution route at room temperature [29]. Flower-like ZnO having 200–500 nm petals composed of nanoparticles and floral assemblies of ZnO nanorods with diameters 100–500 nm had been synthesized by a hydrothermal method [8]. 3D flowerlike ZnO arrays were fabricated by combining laser direct writing and hydrothermal method in which a single nanoflower is composed of many thin nanopetals having thickness of 100 nm [21].

3.2 Structural

The XRD pattern of the syntheised ZnO NFs exhibits peaks along (100), (002), (101), (102), (110), (103), (200), (112), (201), (004), (202) and (104) planes, as shown in Fig. 3, which confirm the formation of hexagonal wurtzite structure of ZnO with polycrystalline nature. The major peaks are along (100), (002) and (101) planes and preferred orientation is along (101) plane. The sharpness of the diffraction peaks indicates good crystallinity of the synthesized ZnO nanostructures.

The absence of any other diffraction peak corresponding to Zn, $Zn(OH)_2$ or other ZnO phase confirms the formation of ZnO with pure hexagonal phase. The crystallite size t_{DS} is estimated using well known Scherrer equation $t_{DS} = 0.9\lambda/(\beta \cos\theta)$, where λ (= 1.540598 Å) is the wavelength of CuK_α radiation and β is the full width at half maximum (FWHM) of the peaks along (hkl) planes. The crystallite size corresponding to major peaks lies between 55 and 59 nm. The lattice constants 'a' and 'c' are calculated using the relation $a = (2/\sqrt{3})d_{(100)}$ and $c = 2d_{(002)}$ [30] and are very near to those of bulk ZnO (a = 3.249 Å and c = 5.205 Å), Table 1.

The variation in lattice parameter compared with strain-free ZnO powder is clear evidence of the presence of strain in the sample. The strain due to crystal imperfection and distortion is calculated using the Wilson formula [31] $\beta = 4\varepsilon\tan\theta$, where β, θ and ε are FWHM, diffraction angle and strain corresponding to specific (hkl) plane. The estimated strain values are given in Table 1. As the sample here is substrate-free and in powder form so the question of lattice mismatch does not arise and the strain present can be attributed to the defects viz. zinc or oxygen vacancies during formation of the nanoflowers. In an ideal stoichiometric wurtzite structure the c/a ratio is 1.633. The sample, here, shows significantly smaller c/a ratio, which also indicates the presence of defects.

XRD patterns for nanosheets and randomly oriented nanorods are similar to each other showing several diffraction peaks which are well known to be indicative of polycrystalline structure whereas vertically aligned nanorods and single crystalline thin films show only one peak, (002) in case of ZnO.

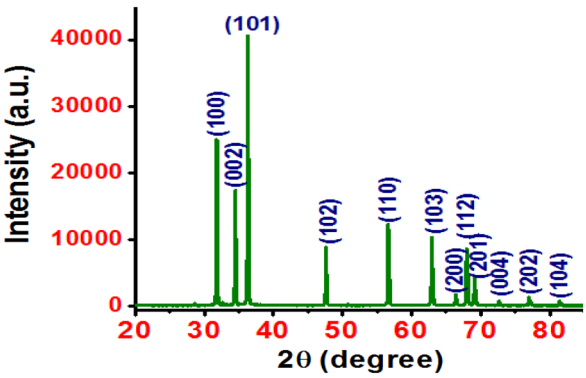

Fig. 3 XRD pattern of the ZnO NFs

3.3 Absorption and optical band gap

The synthesized flower-like ZnO nanostructured powder was dispersed in ethanol in order to record the UV–Vis absorption spectrum. The absorption spectrum obtained here, Fig. 4a, illustrates a strong absorption peak in the UV region at around 395 nm which is a characteristic peak of ZnO [32]. Absorption peak near 380 nm for ZnO NFs may be attributed to the intrinsic band gap absorption of ZnO due to the direct transition of electrons between the valance band and conduction band [8, 29]. Zhang et al. [12] observed absorption peaks at 373 nm, 372 nm and 367 nm corresponding to flower-like, disk-like and nanoflower of nanorod-like petals respectively where the ZnO nanostructures were synthesised using citric acid assisted hydrothermal method. Umar et al. [10] and Mousavi et al. [13] reported absorption peaks for ZnO NFs at 375 nm and 355.5 nm synthesized by hydrothermal and modified sol–gel method, respectively.

The UV–Vis absorption data is used to estimate the optical band gap of ZnO by two different approaches. Firstly extrapolating the linear portion of Tauc's plot $((\alpha h\nu)^2$ vs hν, where α is the absorption coefficient and hν is the photon energy) to the zero ordinate [30], shown in the inset of Fig. 4a. The dashed line represents the extrapolation of the linear region of Tauc plot, the solid curve. The optical band gap of the ZnO NFs is determined to be 3.26 eV. In the second method [33, 34] optical band gap is estimated from the peak position of the curve in the plot (dA/dλ) vs λ, where dA/dλ is the first derivative of the absorbance with respect to the wavelength λ, Fig. 4b. The dominant peak corresponding to optical band gap, Fig. 4b, is observed at 381 nm (3.25 eV). The optical band gap estimated from both methods is nearly same and is smaller than that for bulk ZnO (3.37 eV). Such a red shift in band gap value compared to that for bulk material may be attributed to planar defects

Table 1 Crystallite size, lattice constants and strain of the ZnO NFs with rod-like petals

Sample	t_{DS} (nm)			Lattice constants			Strain ε ($\times 10^{-3}$)		
	(100)	(002)	(101)	a (Å)	c (Å)	c/a	(100)	(002)	(101)
ZnO NFs	58.53	57.19	55.10	3.248	5.201	1.601	2.16	2.05	2.02

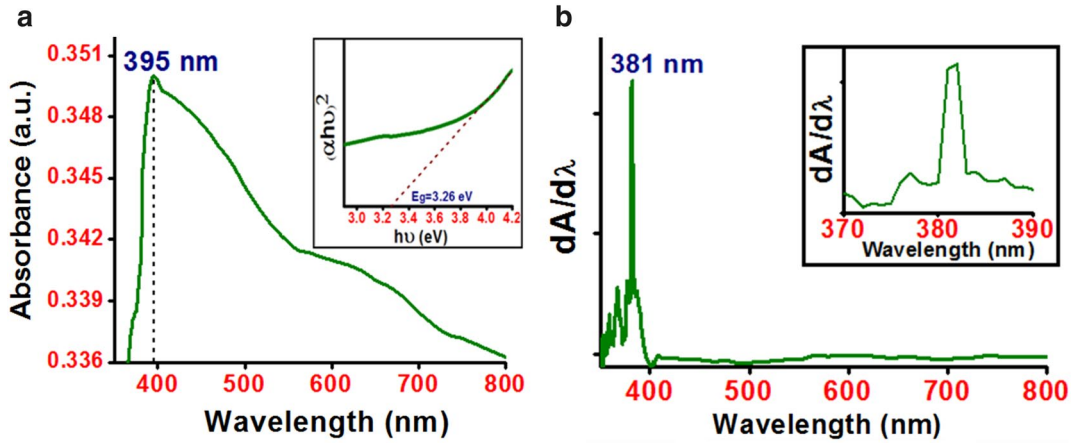

Fig. 4 **a** UV–Vis absorption spectrum of ZnO NFs in the wavelength range 350–800 nm and **b** first derivative of the absorbance with respect to wavelength. Inset of **a** the Tauc's plot and that of **b** enlarged view of the peak corresponding to optical band gap

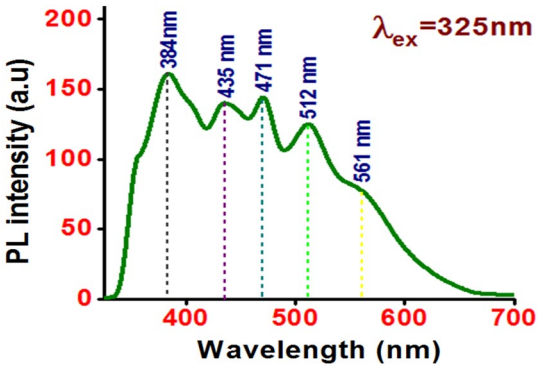

Fig. 5 PL spectrum of ZnO NFs using excitation wavelength of 325 nm

like stacking faults, twin boundaries and intrinsic defects found in ZnO [35]. The optical band gap reported earlier by different researchers is 3.23 eV, 3.40 eV and 3.27 eV for ZnO NFs synthesized by hydrothermal [6], modified sol–gel [13] and solution route [29] method, respectively. The optical band of ZnO nanostructures with different morphologies as nanoflower, nanorods, nanoprisms and nanopyramids using microwave irradiation has been estimated as 3.47 eV, 3.48 eV, 3.45 eV and 3.43 eV, respectively [5].

3.4 Photoluminescence

The room temperature photoluminescence (PL) emission spectrum of the ZnO NFs recorded with an excitation wavelength of 325 nm is shown in Fig. 5. The PL spectrum exhibits a near-band-edge emission (NBE) related UV emission and deep-level emission (DLE) related visible emission. The UV emission centered at 384 nm originates from the radiative recombination of free exciton–exciton collision process in ZnO [36]. The energy of UV emission from our ZnO NFs agrees well with those reported by earlier workers for the ZnO nanostructures grown by hydrothermal method [37]. UV emissions at 380 nm [26], 382 nm [38], and 392 nm [6] have also been reported for flower-shaped ZnO nanostructures. Further, three peaks correspond to visible emission centered at 435 nm (violet emission), 471 nm (blue–green emission) and 512 nm (green emission). A shoulder at 561 nm (yellow emission) is also observed. The UV emission peak is more intense in comparison with other detected peaks indicating the good crystalline quality of ZnO NFs.

Intrinsic defects such as oxygen vacancy (V_O), zinc vacancy (V_{Zn}) and zinc interstitial (Zn_i) are responsible for emissions in the visible region of the electromagnetic spectrum. The radiative transitions involving the energy levels of the defects within the band gap describe the source of defect-emission or visible-emission. The violet emission can be assigned to transition of an electron from a shallow donor level of neutral Zn_i to the top level of the valence band and the blue-green emission may be related to an electron transition from the shallow donor level of Zn_i to an acceptor level of neutral V_{Zn} [39]. The green emission can be considered to correspond to oxygen vacancies (V_O) which are easily formed due to low formation enthalpy [40]. The yellow emission is most common in the hydrothermal growth of ZnO due to the presence of hydroxyl groups [4]. It has been reported earlier that visible emission related to the defect states from the ZnO NFs were negligible compared to UV emission [6]. Wahab et al. [26] reported dominant UV emission at 380 nm and a suppressed broad band emission at 515 nm for ZnO NFs achieved by the solution process.

4 Conclusion

In conclusion, ZnO nano-rods-flowers (NFs) are successfully synthesized with large yield using ultrasonic-assisted hydrothermal method. Moreover, assistance of any template, substrate or seed/buffer layer has not been taken. A simple change i.e. use of inexpensive Borosil autoclave bottle instead of Teflon-coated one provides much economic way to synthesize ZnO NFs/nanostructures with good crystalline quality at low temperature of 95 °C. ZnO NFs, here, show a hexagonal wurtzite phase preferentially oriented along the (101) plane. The optical band gap by two different methods is found to be ~ 3.26 eV. Photoluminescence study of the ZnO NFs shows UV, violet, blue-green, green and yellow emissions and provides an evidence for the existence of defect states. Thus large yield of good-quality ZnO NFs with a band gap tuning of 110 meV with respect to bulk ZnO has been obtained which is a nanostructure comprising of nanostructures (nanorod petals). The significantly high surface area, high crystalline quality and surface defects of ZnO nano-rods-flowers make it more suitable as compared to nano-sheets-flowers for potential applications in various fields especially in gas sensing, antimicrobial activity, non-enzymatic glucose sensor and photodegradation.

Acknowledgements The authors are grateful to Centre of Excellence Scheme of U.P. State Government, Lucknow, India for providing XRD facility at the Department of Physics, University of Lucknow.

Funding The authors are grateful to Centre of Excellence Scheme of U.P. State Government, Lucknow, for providing XRD facility, to DST New Delhi for providing UV–Vis–NIR spectrometer facility (vide Project No. SR/S2/CMP_0028/2010) and to UGC through SAP for providing Fluorescence spectrometer facility at the Department of Physics, University of Lucknow.

Compliance with ethical standards

Conflict of interest The authors declare that they have no conflict of interest.

References

1. Misra KP, Shukla RK, Srivastava A, Srivastava A (2009) Blueshift in optical band gap in nanocrystalline $Zn_{1-x}Ca_xO$ films deposited by sol-gel method. Appl Phys Lett 95:031901
2. Kumar N, Srivastava A (2018) Green photoluminescence and photoconductivity from screen-printed Mg doped ZnO films. J. Alloys Compd. 735:312–318
3. Wang ZL (2004) Nanostructures of zinc oxide. Mater Today 7:26–33
4. Qiu J, Li X, He W, Park SJ, Kim HK, Hwang YH, Lee JH, Kim YD (2009) The growth mechanism and optical properties of ultralong ZnO nanorod arrays with a high aspect ratio by a preheating hydrothermal method. Nanotechnology 20:155603
5. Ahmed F, Arshi N, Anwar MS, Danisha R, Koo BH (2014) Morphological evolution of ZnO nanostructures and their aspect ratio-induced enhancement in photocatalytic properties. RSC Adv 4:29249
6. Vinod R, Sajan P, Achary SR, Tomas CM, Munoz-Sanjose V, Bushiri MJ (2010) Enhanced UV emission from ZnO nanoflowers synthesized by the hydrothermal process. J Phys D Appl Phys 45:425103
7. Lai Y, Meng M, Yu Y, Wang W, Ding T (2011) Photoluminescence and photocatalysis of the flower-like nano-ZnO photocatalysts prepared by a facile hydrothermal method with or without ultrasonic assistance. Appl Catal B 105:335–345
8. Agarwal S, Rai P, Gatell EN, Llobet E, Guell F, Kumar M, Awasthi K (2019) Gas sensing properties of ZnO nanostructures (flowers/rods) synthesized by hydrothermal method. Sens Actuators, B 292:24–31
9. Zhu L, Li Y, Zeng W (2018) Hydrothermal synthesis of hierarchical flower-like ZnO nanostructure and its enhanced ethanol gas-sensing properties. Appl Surf Sci 427:281–287
10. Umar A, Akhtar MS, Al-Hajry A, Al-Assiri MS, Almehbad NY (2012) Hydrothermally grown ZnO nanoflowers for environmental remediation and clean energy applications. Mater Res Bull 47:2407–2414
11. Liang S, Zhu L, Gai G, Yao Y, Huang J, Ji X, Zhou X, Zhang D, Zhang P (2014) Synthesis of morphology-controlled ZnO microstructures via a microwave-assisted hydrothermal method and their gas-sensing property. Ultrason Sonochem 21:1335–1342
12. Zhang H, Yang D, Li S, Ma X, Ji Y, Xu J, Que D (2005) Controllable growth of ZnO nanostructures by citric acid assisted hydrothermal process. Mater Lett 59:1696–1700
13. Mousavi SF, Davar F, Loghman-Estarki MR (2016) Controllable synthesis of ZnO nanoflowers by the modified sol–gel method. J Mater Sci Mater Electron 27:12985–12995
14. Shi Y, Zhu C, Wang L, Li W, Cheng C, Ho KM, Fung KK, Wang N (2012) Optimizing nanosheet-based ZnO hierarchical structure through ultrasonic-assisted precipitation for remarkable photovoltaic enhancement in quasi-solid dye-sensitized solar cells. J Mater Chem 22:13097–13103
15. Ahmadi M, Dafeh SR (2016) Electrical and optical study of ultrasonic-assisted hydrothermal synthesized Ga doped ZnO nanorods for polymer solar cell application. Indian J Phys 90:895–901
16. Chen HF, Wei GD, Han X, Li S, Wang PP, Chubik M, Gromov A, Wang ZP, Han W (2011) Large-scale synthesis of hierarchical alpha-FeOOH flowers by ultrasonic-assisted hydrothermal route. J Mater Sci Mater Electron 22:252–259
17. Zhang JJ, Guo EJ, Yue HY, Wang LP, Zhang CY, Chang J, Gao X (2013) Fabrication of novel hierarchical ZnO via ultrasonic assisted hydrothermal route and their gas sensing property. J Mater Sci Mater Electron 24:3435–3441
18. Fan J, Li T, Heng H (2016) Hydrothermal growth of ZnO nanoflowers and their photocatalyst application. Bull Mater Sci 39:19–26
19. Kilic B, Gunes T, Besirli I, Sezginer M, Tuzemen S (2014) Construction of 3-dimensional ZnO-nanoflower structures for high quantum and photocurrent efficiency in dye sensitized solar cell. Appl Surf Sci 318:32–36
20. Kansal SK, Ali AH, Kapoor S, Bahnemann DW (2011) Synthesis of flower like zinc oxide nanostructure and its application as a photocatalyst. Sep Purif Technol 80:125–130
21. Guo X, Zhao Q, Li R, Pan H, Guo X, Yin A, Dai W (2010) Synthesis of ZnO nanoflowers and their wettabilities and photocatalytic properties. Opt Express 18:18401

22. Xu Y, Jin J, Li X, Han Y, Meng H, Wang T, Zhang X (2016) Simple synthesis of ZnO nanoflowers and its photocatalytic performances toward the photodegradation of metamitron. Mater Res Bull 76:235–239
23. Umar A, Chauhan MS, Chauhan S, Kumar R, Sharma P, Tomar KJ, Wahab R, Al-Hajry A, Singh D (2013) Applications of ZnO Nanoflowers as antimicrobial agents for escherichia coli and enzyme-free glucose sensor. J Biomed Nanotechnol 9:1794–1802
24. Kong XY, Wang ZL (2004) Polar-surface dominated ZnO nanobelts and the electrostatic energy induced nanohelixes, nanosprings, and nanospirals. Appl Phys Lett 84:975–977
25. Zhang Z, Mu J (2007) Hydrothermal synthesis of ZnO nanobundles controlled by PEO–PPO–PEO block copolymers. J Colloid Interface Sci 307:79–82
26. Wahab R, Ansari SG, Kim YS, Seo HK, Kim GS, Khang G, Shin HS (2007) Low temperature solution synthesis and characterization of ZnO nano-flowers. Mater Res Bull 42:1640–1648
27. Zhang X, Qin J, Xue Y, Yu P, Zhang B, Wang L, Liu R (2014) Effect of aspect ratio and surface defects on the photocatalytic activity of ZnO nanorods. Sci Rep 4:4596
28. Bai X, Wang L, Zong R, Zhu Y (2013) Photocatalytic activity enhanced via g-C3N4 nanoplates to nanorods. J Phys Chem C 117:9952–9961
29. Wang Y, Ma Q, Kong J, Jia H, Wang Z (2015) Solution self-assembly of flower-like ZnO nanostructures with nanosheets and their optical properties. Mater Technol Adv Perform Mater 31:13–17
30. Srivastava A, Kumar N, Khare S (2014) Enhancement in UV emission and band gap by Fe doping in ZnO thin films. Opto Electron Rev 22:68–76
31. Williamson GK, Hall WH (1953) X-ray line broadening from filed aluminium and wolfram. Acta Metall 1:22–31
32. Sadhukhan P, Kundu M, Rana S, Kumar R, Das J, Sil PC (2019) Microwave induced synthesis of ZnO nanorods and their efficacy as a drug carrier with profound anticancer and antibacterial properties. Toxicol Rep 6:176–185
33. Saha B, Sarkar K, Bera A, Deb K, Thapa R (2017) Schottky diode behaviour with excellent photoresponse in NiO/FTO heterostructure. Appl Surf Sci 418:328–334
34. Henríquez R, Grez P, Muñoz E, Gómez H, Badán JA, Marotti RE, Dalchiele EA (2010) Optical properties of CdSe and CdO thin films electrochemically prepared. Thin Solid Films 518:1774–1778
35. Jangir LK, Kumari Y, Kumar A, Kumar M, Awasthi K (2017) Investigation of luminescence and structural properties of ZnO nanoparticles, synthesized with different precursors. Mater. Chem. Front. 1:1413–1421
36. Hameed ASH, Karthikeyan C, Ahamed AP, Thajuddin N, Alharbi NS, Alharbi SA, Ravi G (2016) In vitro antibacterial activity of ZnO and Nd doped ZnO nanoparticles against ESBL producing *Escherichia coli* and *Klebsiella pneumoniae*. Sci Rep 6:24312
37. Pal U, Santiago P (2005) Controlling the morphology of ZnO nanostructures in a low-temperature hydrothermal process. J Phys Chem B 109:15317–15321
38. Fang Z, Tang K, Shen G, Chen D, Kong R, Lei S (2006) Self-assembled ZnO 3D flowerlike nanostructures. Mater Lett 60:2530–2533
39. Kumar N, Srivastava A (2018) Enhancement in NBE emission and optical band gap by Al doping in nanocrystalline ZnO thin films. Opto-Electron Rev 26:1–10
40. Katiyar A, Kumar N, Srivastava A (2018) Optical properties of ZnO nanoparticles synthesized by co-precipitation method using LiOH. Mater Today Proc 5:9144–9147